Journal of Alloys and Compounds 824 (2020) 153972

Contents lists available at ScienceDirect

Journal of Alloys and Compounds

journal homepage: http://www.elsevier.com/locate/jalcom

Wetting and interfacial behavior of Cu–Al/SiC systems: Influences of Si ion implantation and Al concentration

Yalong Zhu [a, b], Mingfen Zhang [a], Xiangzhao Zhang [a, **], Zhikun Huang [a, c], Guiwu Liu [a, b, *], Guanjun Qiao [a]

[a] School of Materials Science and Engineering, Jiangsu University, Zhenjiang, 212013, China
[b] School of Mechanical and Electrical Engineering, Xinyu University, Xinyu, 338000, China
[c] State Key Laboratory of Chemical Engineering, College of Chemical and Biological Engineering, Zhejiang University, Hangzhou, 310027, China

ARTICLE INFO

Article history:
Received 31 October 2019
Received in revised form
14 January 2020
Accepted 20 January 2020
Available online 22 January 2020

Keywords:
SiC
Ion implantation
Wetting
Interfaces

ABSTRACT

Three doses (5×10^{15}, 1×10^{16} and 5×10^{16} ions/cm^2) of Si ions implantation into Si-terminated 6H–SiC substrate were carried out at an energy of 20 keV at room temperature. The wetting of pristine and Si-implanted 6H–SiC (Si–SiC) substrates by molten pure Cu, Cu-(42.9, 48.7, 70.4)Al alloys and pure Al were performed by the sessile drop technique under vacuum of ~4×10^{-4} Pa at 1373 K. The surface characteristics of SiC substrates and wetting and interfacial behavior of Cu–Al/(Si-)SiC systems were analyzed and discussed. The equilibrium or final contact angles (θ) of Cu–Al/Si–SiC systems were increased more or less with the increase of Si ion implantation dose, and the Si ion implantation can markedly enhance the wettability of Cu-(0, 42.9)Al/SiC systems but weaken that of Cu-(48.7, 70.4, 100)Al/SiC systems. Interestingly, the graphitization phenomenon disappeared at the drop/substrate interface when the Al concentration was over 42.9%, and the Cu-42.9Al alloy cannot wet both the pristine 6H–SiC and Si–SiC substrates. These phenomena further demonstrated that the wetting of metal/SiC systems can be mainly determined by the metal-substrate interactions derived from the metal composition under a vacuum of and surface characteristics of metal drop and ceramic substrate during wetting.

1. Introduction

Silicon carbide (SiC), as a kind of promising structure-function integrated material, has been extensively used in high-temperature structural ceramic components, semiconductor devices, and SiC reinforced metal matrix composites [1–3]. The manufacturing processes in those applications are closely related to wettability and interfacial behavior of molten metals on SiC [4–8]. For instance, the directional SiC/Cu–Si composite as promising heat sink material was fabricated by spontaneous infiltration based on the good wettability of non-reactive Cu–24Si/SiC system [9]. To reveal the wetting and interfacial behavior of molten Al and Cu on SiC substrates, many researchers performed diverse investigations. For instance, Shen et al. reported the wetting of polycrystalline SiC by molten Al at 1123–1273 K, and found that the wetting was controlled by the deoxidation of SiC substrate surface firstly and then by the formation of Al_4C_3 at the interface [10]. Moreover, an Al_4C_3 layer was generated at the Al/Si-terminated SiC interfaces after dwelling at 973–1173 K for 2 h, especially it was discontinuous at 973 K but became almost fully dense at 1023–1173 K [11]. In particular, we summarized the wettability of molten Al on SiC [12], indicating that the wettability was closely related to the measured temperature, chemical composition and surface polarity of SiC substrate. On the other hand, Rado et al. reported the wetting of molten Cu on Si-terminated 6H–SiC substrate at 1373 K for 50 min, and confirmed that a graphite layer acting as a barrier to wetting was generated, resulting in the slower spreading and higher contact angle [13]. In fact, the addition of Cu into Al can affect the interfacial reactions and final contact angle of molten Al on SiC. For instance, An et al. investigated the effect of Cu addition (2.2–6.9 at.%) on the wettability of molten Al on polycrystalline α-SiC substrate at 1173 K, and found that the addition of Cu slightly deteriorated the wettability and decreased the spreading rate but alleviated the formation of Al_4C_3 due to the decrease of activity of Al

* Corresponding author. School of Materials Science and Engineering, Jiangsu University, Zhenjiang, 212013, China.
** Corresponding author.
E-mail addresses: xzzhang2018@ujs.edu.cn (X. Zhang), gwliu76@ujs.edu.cn (G. Liu).

https://doi.org/10.1016/j.jallcom.2020.153972
0925-8388/

[14].

As we know, ion implantation can cause a series of changes in physical and chemical properties of SiC monocrystal substrate surface, such as introducing impurity atoms of metal, generating free C and Si atoms and producing surface vacancy defects, resulting in an increase of solid-vapor surface energy (σ_{SV}) of SiC substrate [[12], [15–17]]. Based on these changes and the potential advantages of ion implantation process, recently our group focused on investigating the influences of metal ions implantation on the wettability of metal/SiC systems. For instance, Zhao et al. [15] investigated the influence of Mo ion implantation (3.5×10^{17} ions/cm^2) on the wettability of reactive Ni/SiC system and non-reactive Ni−56Si/SiC system before and after succeeding annealing treatments, indicating that the improvement of wettability was mainly attributed to the increase of σ_{SV} and to the presence of Mo on the SiC substrate derived from the Mo ion implantation. Huang et al. [[12], [17–19]] studied the influence of Pd ion implantation (5×10^{15}–5×10^{17} ions/cm^2) on Al−Si-X(X = Cu, Mg and Zn)/6H−SiC systems, and confirmed that the Pd ion implantation can obviously enhance the wettability of molten Si, Al-(5, 10, 12)Si and Al−10Si−4Cu alloys on SiC and deteriorate that of molten Al and Al−12Si−2Mg and hardly affect that of molten Al-(20, 30)Si and Al−10Si−10Zn alloys.

As discussed above, the distinguishable interfacial behavior (*i.e.*, the formation of graphite layer or Al_4C_3) can be detected at the Cu, Al or Al-based alloys/SiC interface, depending on the drop compositions. However, the effect of Al addition on the wetting and interfacial behavior of Cu/SiC system is less investigated. Thus, we selected pure Cu, Al and Cu-(42.9, 48.7, 70.4)Al alloys (all in at.% in this text) as drops for wetting of SiC substrate based on interfacial reactivity of Cu−Al/SiC systems, and selected Si as ion implantation source for no introducing additional impurity atom and keeping the semiconductor characteristic of SiC substrate as possible. Moreover, the variations of wetting (wettability and spreading) and interfacial behavior were analyzed and discussed as functions of Si ion implantation dose and Al concentration.

2. Experimental procedure

The research-grade double-side chemical-mechanically polished Si-terminated SiC monocrystals (Tankeblue semiconductor Corp., Beijing) were employed as the substrates, with orientation of <0001>±5° and average surface roughness of less than 2 nm [15]. The SiC wafers were mechanically processed into pieces of ~7 mm × 7 mm × 0.33 mm. The pure Cu and Al with a purity of over 99.99% and the commercial Cu-70.4Al alloy with a purity of over 99.9% were used as drops to perform the wetting experiments. Moreover, the Cu-42.9Al and Cu-48.7Al alloys were fabricated by vacuum induction melting for several times using pure Cu and Cu-70.4Al alloy as starting materials, and the chemical compositions of Cu-(42.9, 48.7, 70.4)Al alloys were determined by energy dispersive spectroscopy (EDS) analysis.

The Si ion implantation was performed at energy of 20 keV and three total fluences (5×10^{15}, 1×10^{16} and 5×10^{16} ions/cm^2) at room temperature (RT) under vacuum of ~4×10^{-3} Pa using an ion implanter (MEVVA-36, Beijing), respectively, and the beam density was less than 1 μA/cm^2 during ion implantation. The Monte Carlo software was employed to analyze the distributions of Si, C and their total atomic vacancies and the displacement per atom (dpa) on Si-implanted 6H−SiC (Si−SiC) substrate.

Prior to experiments, pure Cu and Al and Cu-(42.9, 48.7, 70.4)Al alloys were processed into ~1 mm × 1 mm × 1 mm cubic pieces, and then these metals and 6H−SiC substrates were placed in a solution of dilute hydrochloric acid to handle ultrasonic cleaning for 15 min. Subsequently, they were further cleaned up 3 to 5 times by using deionized water, and finally cleaned ultrasonically in ethanol for 15 min. The as-treated metals and 6H−SiC substrates were placed in the wetting furnace (OCA15LHT-SV, Dataphysics, Germany). During the sessile drop experiments, the heating rate was 5 K/min while the peak temperature and holding time were set to be 1373 K and 90−300 min under vacuum of ~4×10^{-4} Pa, respectively, and finally naturally cooled to RT. The average contact angles of metals on the SiC substrates were calculated by designed SCA image analysis software with a precision of ±2° [20]. After the wetting experiments, partial metal/ceramic couples were selected, and some solidified drops were cut down the most part mechanically and then corroded using saturated sodium hydroxide solution until no gas was produced, or some metal/ceramic couples were cut along the cross-section using SYJ-16 low speed diamond cutting machine and then polished using UNIPOL-802 polishing machine. The interfacial microstructures of Cu−Al/(Si-)SiC systems were observed and analyzed by scanning electron microscope (SEM) equipped with EDS.

3. Results and discussion

Fig. 1 presents that the variations of Si, C and their total atomic vacancies and dpa with depth on the Si−SiC substrates. The maximum implantation damage was essentially centered at ~12 nm, and the implantation depth was ~45 nm. The dpa levels were 7.6, 15.0 and 76.7 while implanting at 5×10^{15}, 1×10^{16} and 5×10^{16} ions/cm^2, respectively, demonstrating that the dpa can be affected linearly by the implantation dose. Meanwhile, the number of Si vacancy was more than that of C vacancy in the case of same depth, which can be verified by much higher formation energy of C vacancy than Si vacancy [21].

Fig. 2a shows the Raman spectra of pristine 6H−SiC and Si−SiC substrates. As shown in Fig. 2a, three first-order peaks of Si−C vibration involving two transverse (TO) optical and one longitudinal (LO) optical modes were located at ~766, 788, 967 cm^{-1} on the Si−SiC substrates, respectively, which was in good agreement with precious investigations [22–25]. The peak intensity was reduced with the Si implantation dose increasing, indicating that varying degrees of lattice damage to the 6H−SiC substrate can be produced by the three doses of Si implantation, resulting in the increase of σ_{SV} of SiC substrate. Fig. 2b shows XPS spectra of pristine 6H−SiC and Si−SiC substrates implanted at 5×10^{16} ions/cm^2. As expected, no new peak was observed due to the selection of Si ion source except that the O peak intensity was enhanced. The Si peaks at 100.4 eV and 102.6 eV can be assigned to metallic Si and Si−O, respectively (Fig. 2c) [26], indicating that the Si element on the Si−SiC surface mainly existed as an elementary substance and in the oxidation state. As shown in Fig. 2d, the O peaks at 531.8 eV and 532.5 eV can be assigned to oxygen adsorbed on the SiC substrate and S−O bonding [27,28].

Figs. 3a and 4 show the variations of contact angle with time and the top-view and cross-sectional SEM images of Cu/(Si-)SiC systems. An early stabilization stage was only observed in the case of wetting of molten Cu on the pristine SiC substrate, the contact angle remained almost constant and even increased, and the relatively large initial contact angle of ~134° was mainly attributed to the oxide film (SiO_2) on the pristine SiC surface [29]. Eq. (1) for the removing of oxide film can take place immediately, and then the wetting curve entered into the fast spreading stage where Eq. (2) was carried out to form the graphite. With the prolonging of holding time, the SiC substrate was dissolved and the molten Cu was consumed continuously, as a result of that the graphitization reaction continued to advance. Finally, the Cu/SiC system entered the slow spreading stage with the final contact angle of ~70°. The early stabilization stage disappeared after Si ion implantation,

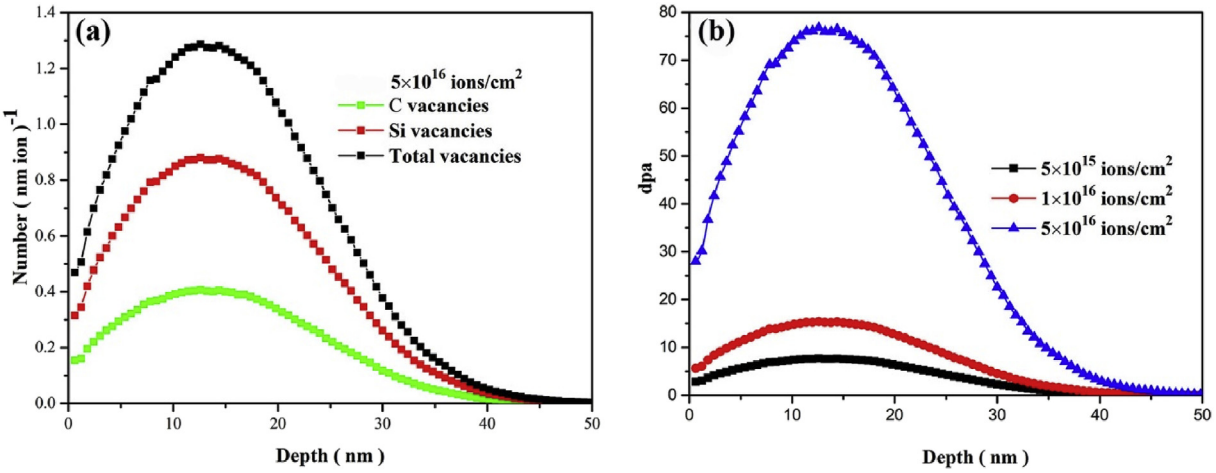

Fig. 1. (a) Variations of Si, C and their total atomic vacancies and (b) dpa with depth on Si−SiC substrate implanted at 5 × 10^{16} ions/cm^2 or the three doses of Si ions.

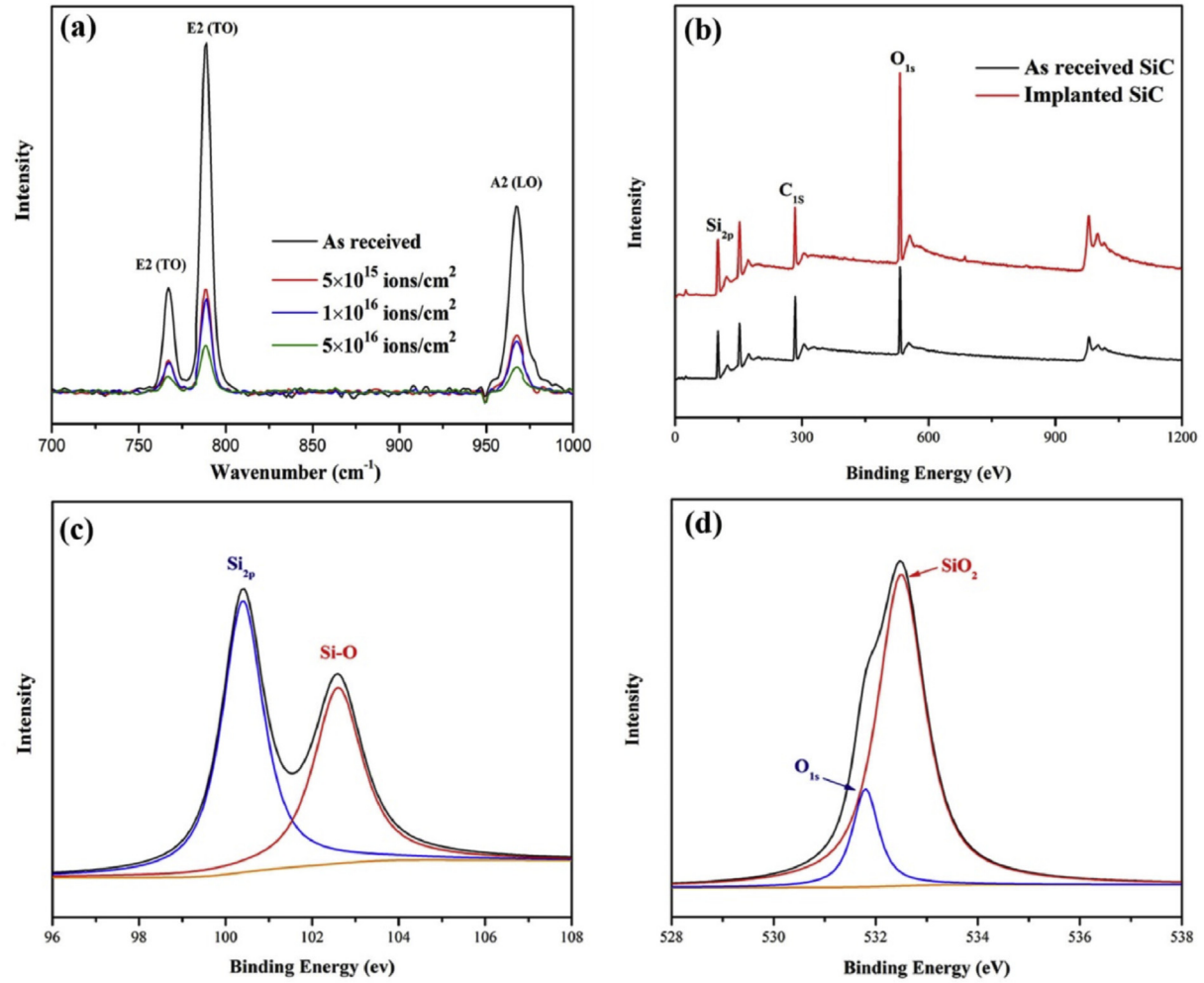

Fig. 2. (a) Raman spectra of pristine 6H−SiC and Si−SiC substrates implanted at 5 × 10^{15}, 1 × 10^{16} and 5 × 10^{16} ions/cm^2, (b) XPS survey spectra of pristine 6H−SiC and Si−SiC substrates implanted at 5 × 10^{16} ions/cm^2 at 20 keV, (c) Si spectrum and (d) O spectrum after Si ion implantation.

which can be related to the accelerated removing of oxide film derived from Eqs. (1) and (3). As shown in Fig. 3a, the equilibrium contact angle decreased greatly from ~70° to ~25° after the Si implantation of 5 × 10^{15} ions/cm^2. However, the equilibrium contact angles were increased markedly from ~25° to ~39° with the implantation dose rising from 5 × 10^{15} to 5 × 10^{16} ions/cm^2. Besides, the σ_{SV} of 6H−SiC substrate was increased due to the presence of the vacancies and lattice damage (Figs. 1 and 2a). On the other

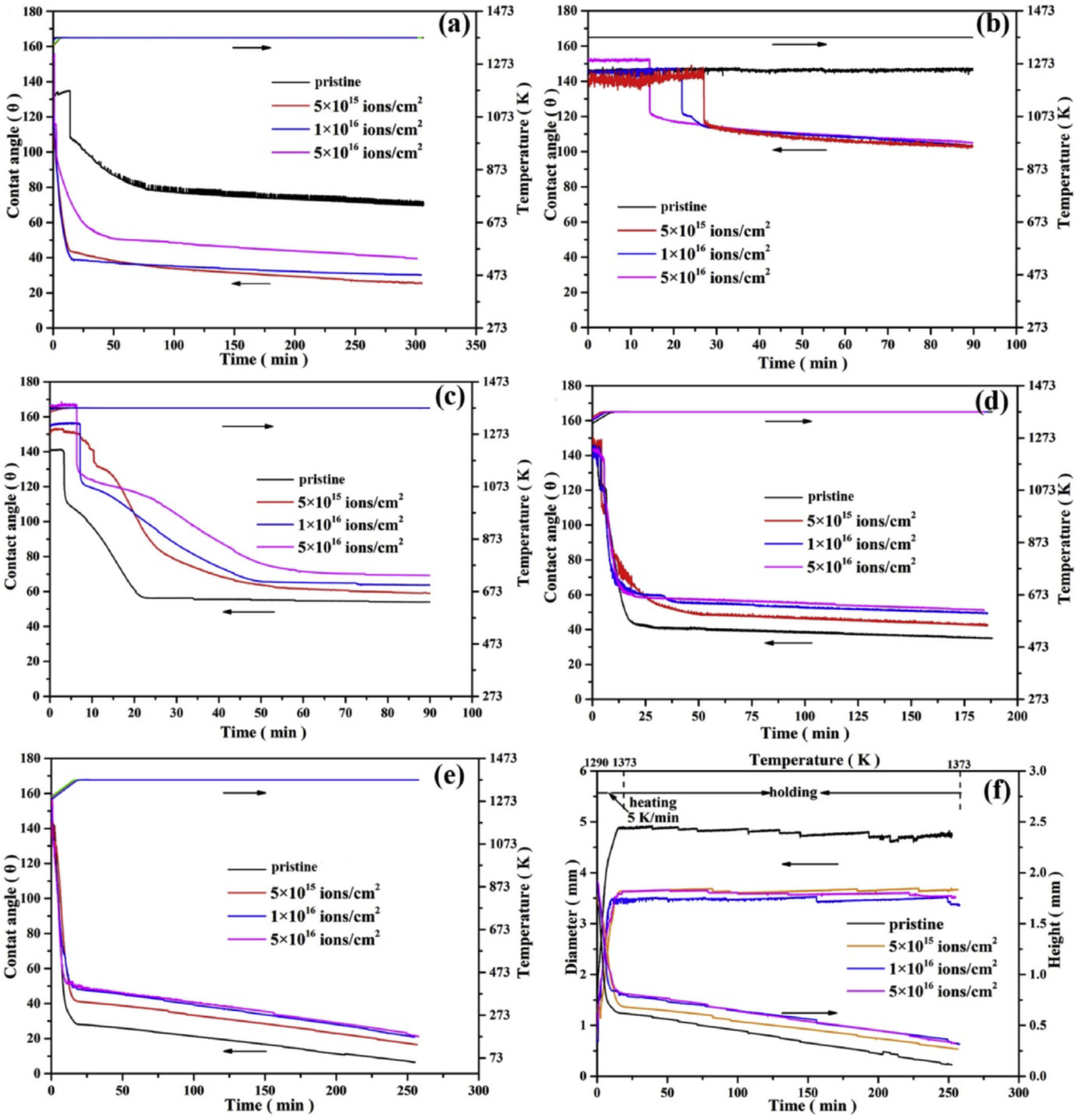

Fig. 3. Variations of contact angle of Cu−Al/(Si-)SiC systems with time at 1373 K: (a) pure Cu, (b) Cu-42.9Al, (c) Cu-48.7Al, (d) Cu-70.4Al and (e) pure Al, and (f) variations of diameter and height of Al/(Si-)SiC systems with time in vacuum at 1373 K.

hand, the early stabilization stage only existed in the Cu/SiC system rather than in Cu/Si−SiC systems (Fig. 3a), and a visible graphite layer increased from ~0.5 mm to ~1 mm in width with the Si ion implantation doses increasing from 5×10^{15} ions/cm^2 to 5×10^{16} ions/cm^2, which was only formed at the triple line region after the Si ion implantation (Fig. 4b1–d1). Moreover, two diverse scallops were formed due to the inconsistent interfacial interactions between Cu and SiC substrate (Fig. 4a3 and b3), indicating the aggravated consumption of SiC substrate after the Si ion implantation. In particular, the laminated graphite layer at the drop/substrate interface firstly became dense and then sparse gradually (Fig. 4a2–d2), indicating that the interfacial interactions were firstly strengthened markedly and then weakened gradually, resulting in the decrease of solid-liquid interfacial energy (σ_{SL}) more or less. Actually, the trace Si originated from the ion implantation can enter into the lattice of SiC crystal and thus induced the lattice damage, which can give rise to the variation of contact angle derived from the changes of σ_{SV} and σ_{SL} rather than the

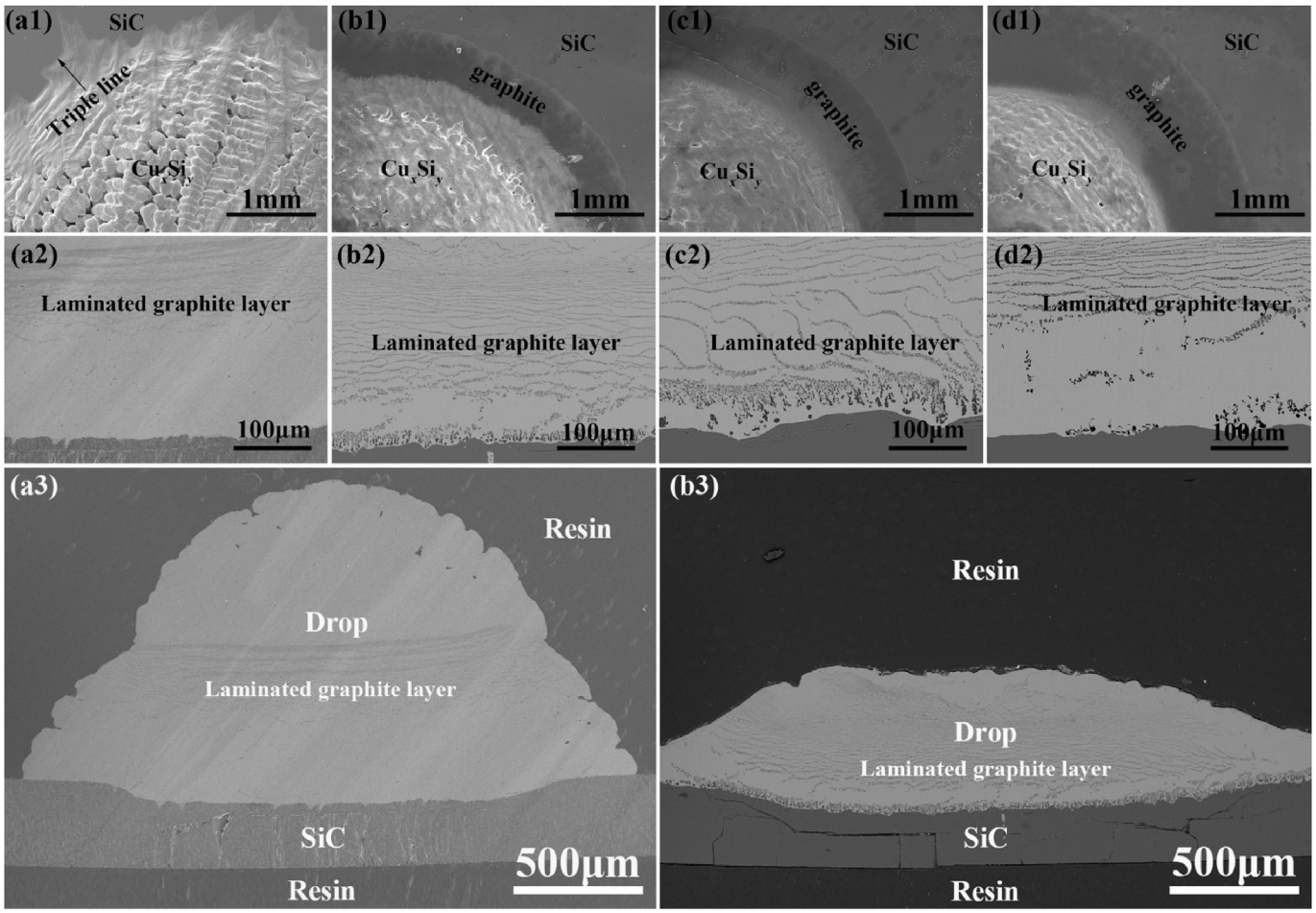

Fig. 4. Top-view and cross-sectional SEM images of Cu/SiC systems (a) before and (b–d) after Si ion implantation of 5×10^{15}, 1×10^{16} and 5×10^{16} ions/cm^2 at 1373 K: (a1–d1) at the triple line, (a2–d2) cross-sections at the central interfaces, (a3, b3) lower-magnification cross-sections of Cu/SiC couples.

variation of interfacial reaction type. Therefore, we can conclude that the equilibrium contact angle was firstly reduced greatly and then climbed gradually based on the Young's equation $\cos\theta = (\sigma_{SV} - \sigma_{SL})/\sigma_{LV}$ on the condition that the liquid–vapor surface energy (σ_{LV}) kept invariant.

$$2SiO_2\,(film) + SiC \rightarrow 3SiO_{(g)}\uparrow + CO\,(g)\uparrow \quad (1)$$

$$xCu_{(l)} + ySiC_{(S)} \leftrightarrow Cu_xSi_y + yC \quad (2)$$

$$Si + SiO_2\,(film) \rightarrow 2SiO_{(g)}\uparrow \quad (3)$$

Figs. 3b and 5 show the variations of contact angle of Cu-42.9Al/(Si-)SiC systems with time and the cross-sectional microstructures before and after Si ion implantation of 5×10^{15} ions/cm^2, respectively. The molten Cu-42.9Al alloy hardly spread on pristine SiC substrate during the holding, and the contact angle was kept a constant value of ~143°, which can be mainly attributed to the oxide film (Al_2O_3) on the surface of drop (Fig. 5a1). And the passive oxide film on the drop surface cannot be ruptured because of the relatively low activity of Al element in Cu-42.9Al alloy, namely Eq. (4) cannot occur well. The time of duration in the early stabilization stage was shortened with the Si ion implantation increasing, deriving from the occurrence of Eq. (3) at different levels [30]. Surprisingly, the Cu-42.9Al alloy still cannot wet the Si–SiC substrate with a stable contact of ~100° (Fig. 5b1), which can be attributed to the intactness of oxide film on the drop surface and the increased viscosity of the drop [31–34]. Corresponding to the no spreading and no wetting, the graphitization phenomenon and interfacial reaction can hardly occur (Fig. 5).

$$4Al_{(l)} + Al_2O_3\,(film) \rightarrow 3Al_2O_{(g)}\uparrow \quad (4)$$

Fig. 3c–e displays the variations of contact angle with time for Cu-(48.7, 70.4, 100)Al/(Si-)SiC systems. Compared with the Cu-42.9Al/SiC system, the early stabilization stage was shorted and till disappeared, while the rapid spreading stage was accelerated gradually, which should be related to the increasing activity of Al in Cu-48.7Al, Cu-70.4Al alloy and pure Al. The equilibrium or final contact angle of Cu–Al/SiC system was increased firstly and then decreased greatly from ~70° to 134°, 50°, 40 and 7° with the Al concentration increasing from 0 to 42.9, 48.7, 70.4 and 100, which can be mainly related to the variation of interfacial interactions between Cu–Al drop and SiC substrate. In this case, the liquid–vapor surface energy (σ_{LV}) decreased and the solid-liquid interfacial energy (σ_{SL}) increased firstly and then decreased derived from the variation of interfacial interactions with the increase of Al concentration, while the solid–vapor surface energy (σ_{SV}) kept invariant. Actually, the σ_{SL} is a more significant factor than the σ_{LV} for reactive wetting of metal/ceramic [12]. So, the contact angle fluctuated greatly according to the Young's equation. Moreover, the equilibrium or final contact angle of Cu–Al/SiC

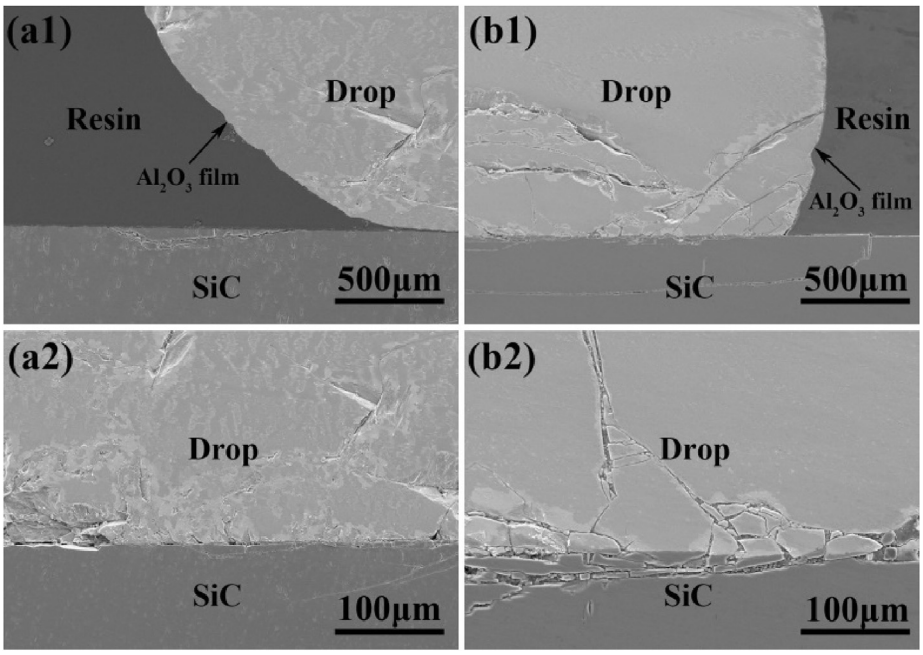

Fig. 5. Cross-sectional microstructures of Cu-42.9Al/SiC systems (a) before and (b) after Si ion implantation of 5×10^{15} ions/cm^2 at 1373 K: (a1, a2) at the triple line, (a2, b2) cross-sections at the central interface.

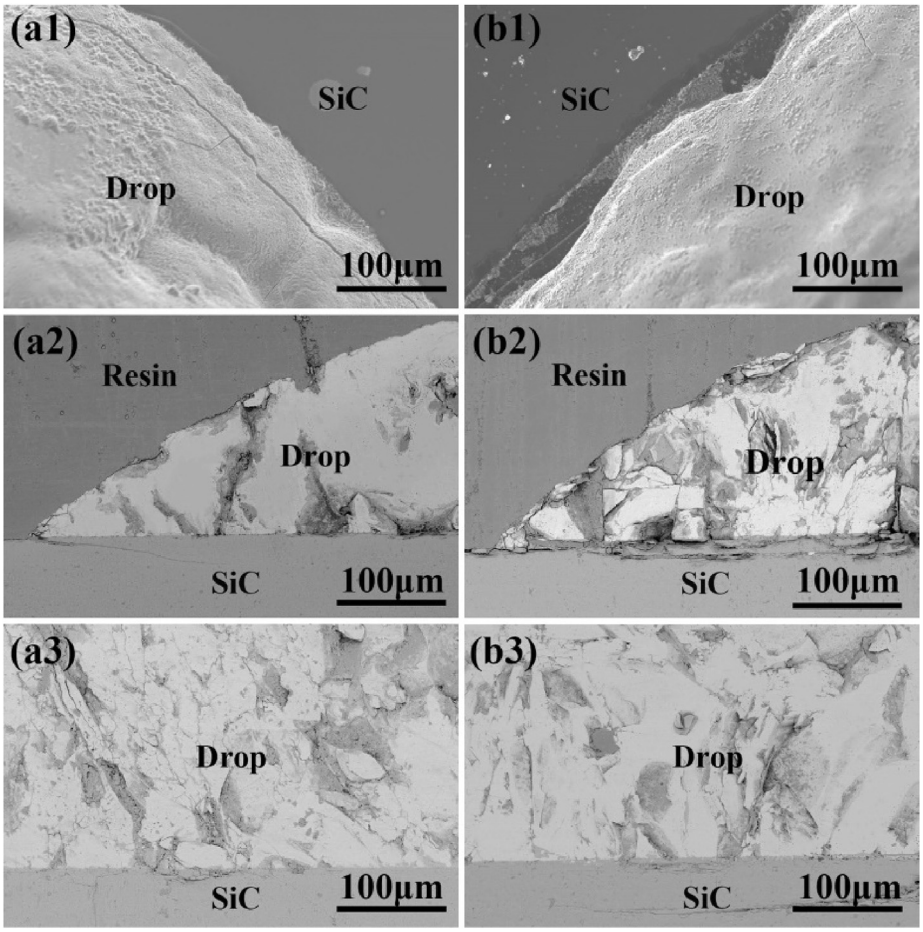

Fig. 6. Interfacial microstructures of Cu-48.7Al/SiC systems (a) before and (b) after Si ion implantation of 5×10^{16} ions/cm^2 at 1373 K: (a1–b2) at the triple line, (a3, b3) cross-sections at the central interface.

systems was increased to varying degrees with the increase of Si implantation dose (Fig. 3a–e). For instance, the equilibrium contact angle of Cu-48.7Al/SiC system was climbed from ~60° to ~64° and ~69° with the Si implantation dose rising from 5×10^{15} to 1×10^{16} and 5×10^{16} ions/cm^2. Surprisingly, different from the two Cu-(0, 42.9)Al/SiC systems, the contact angles of Cu-(48.7, 70.4, 100)Al/Si−SiC systems were higher than those of Cu-(48.7, 70.4, 100)Al/SiC systems, respectively, that is the Si implantation reduced the wettability of Cu-(48.7, 70.4, 100)Al/SiC systems, which can be related with the chemical activity of Al in the drop. Fig. 3f shows the variations of height and diameter of the molten drop in Al/(Si-)SiC systems with time at 1373 K. The height of the molten Al drop was decreased while its diameter remained basically unchanged during the holding stage, indicating that the molten Al gradually evaporated in the vacuum atmosphere due to the low vapor pressure (about 10^{-1} Pa at 1373 K [35]). And the evaporation process can contribute to non-equilibrium states of Al/(Si-)SiC system. Actually, the continuous interfacial reaction and oxide removal also had a certain influence on the spreading.

Fig. 6–8 show the interfacial microstructures of Cu-48.7Al/(Si-)SiC, Cu-70.4Al/(Si-)SiC and Al/(Si-)SiC systems, respectively. Compared with non-reactive interface of the Cu-42.9Al/(Si-)SiC systems, low-reactive and reactive interfaces was formed in the Cu-48.7Al/(Si-)SiC and Cu-70.4Al/(Si-)SiC systems, respectively. A thin Al_4C_3 layer can be observed at the triple line of Cu-48.7Al/SiC system, and a wider Al_4C_3 layer was generated at the advancing contact line of Cu-70.4Al/Si−SiC system (see Eq. (5)). As expected, a dense Al_4C_3 layer was formed at the triple line and at drop/substrate interface of Al/(Si-)SiC systems. Moreover, the Al_4C_3 layer at the triple line became denser and wider, and the Al_4C_3 grains became finer with the implantation dose rising from 0 to 5×10^{16} ions/cm^2. This was mainly attributed to the increased lattice damage (Si and C vacancies) induced by the Si ion implantation. As shown in Fig. 1, the degree of lattice damage increased with the implantation dose rising, resulting in the enhanced active sites for the interfacial reaction (Eq. (5)). In fact, the wider Al_4C_3 layer at the triple line can prevent the molten drop spreading more or less [10].

$$4Al_{(l)} + 3SiC \rightarrow 3Al_4C_{3(s)} + 3Si \quad (5)$$

4. Conclusions

The wetting of molten Cu-(0, 42.9, 48.7, 70.4, 100)Al on pristine 6H−SiC and Si−SiC substrates was investigated, and the influences of Si ion implantation dose (5×10^{15}, 1×10^{16} and 5×10^{16} ions/cm^2) and Al concentration on the wetting (wettability and spreading) and interfacial behavior were analyzed and discussed. The Si ion implantation can produce vacancy defects and lattice damage on the 6H−SiC surface. The Si ion implantation can improve the wettability of Cu-(0, 42.9)Al/SiC systems but reduce that of Cu-(48.7, 70.4, 100)Al/SiC systems. The equilibrium or final contact angle of Cu−Al/SiC systems was enhanced more or less

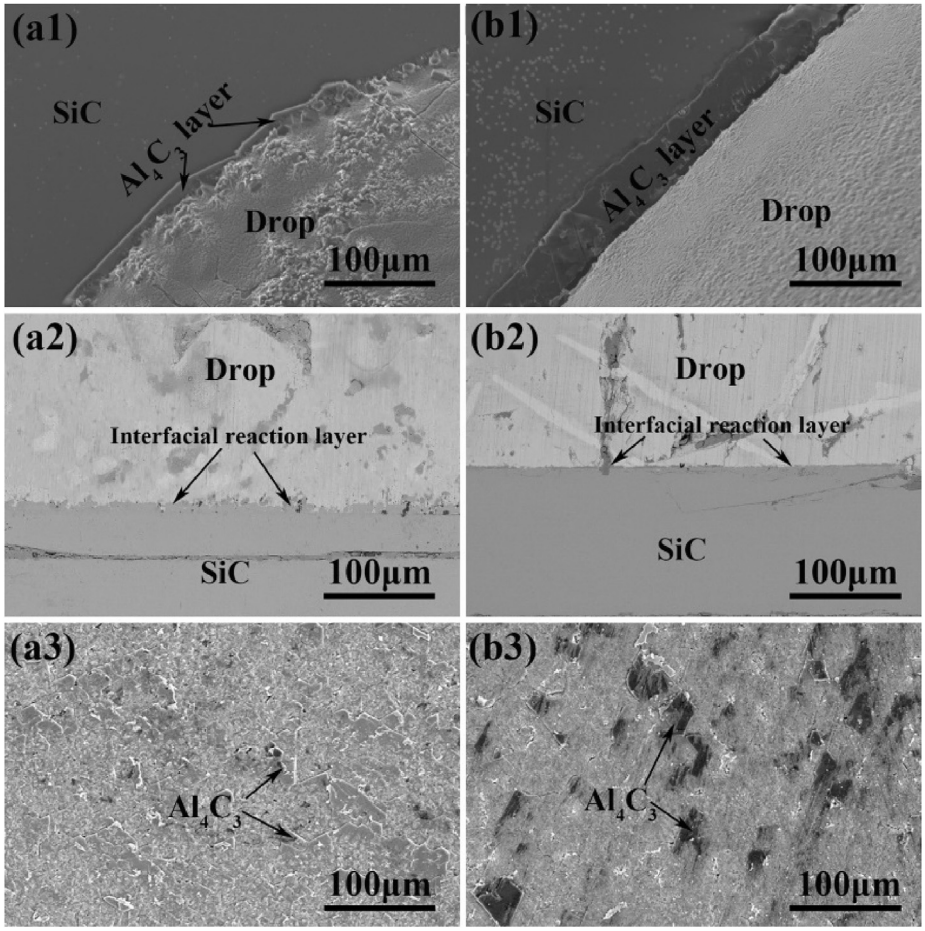

Fig. 7. Interfacial microstructures of Cu-70.4Al/SiC systems (a) before and (b) after Si ion implantation of 5×10^{16} ions/cm^2 at 1373 K: (a1, b1) at the triple line, (a2, b2) cross-sections at the central interface, (a3, b3) at the central interface after removal of the solidified Cu-70.4Al drop.

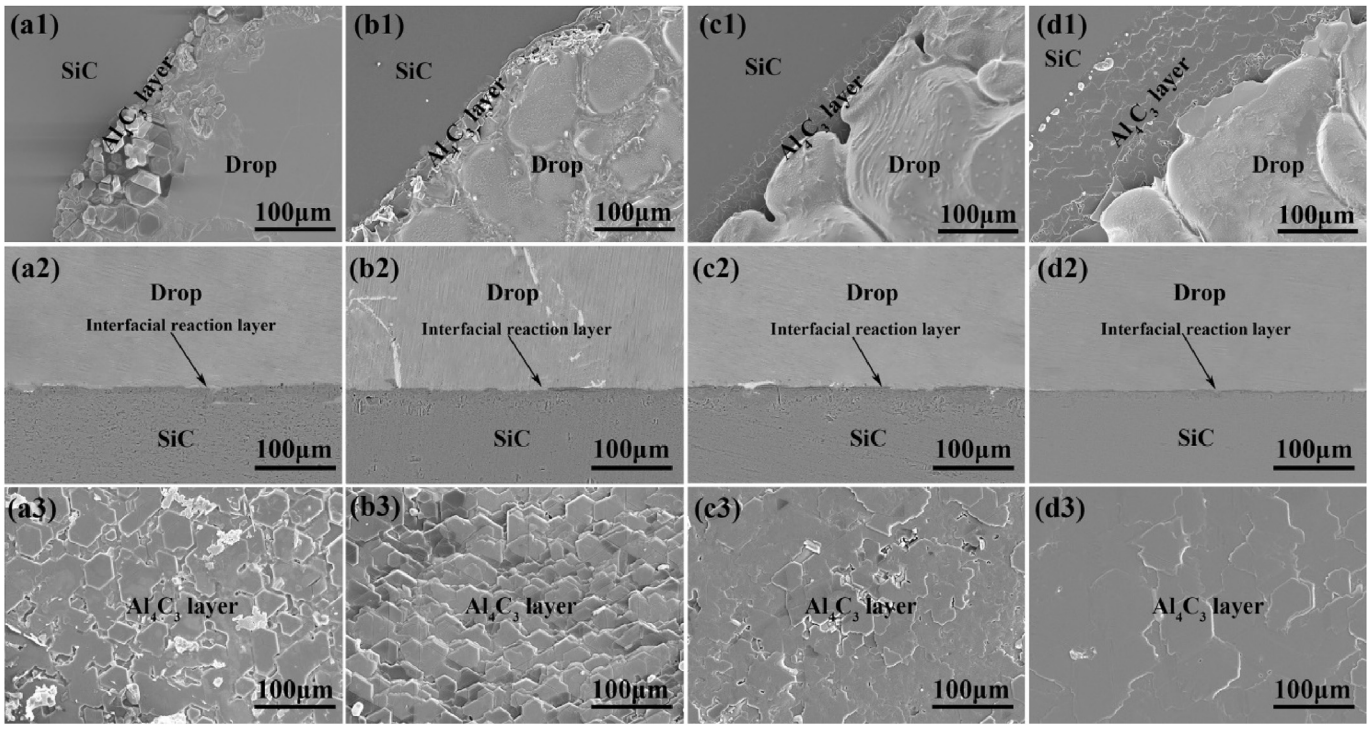

Fig. 8. Interfacial microstructures of Al/Si–SiC systems (a) before and (b–d) after the Si ion implantation of 5×10^{15}, 1×10^{16} and 5×10^{16} ions/cm^2 at 1373 K: (a1–d1) at the triple line, (a2–d2) cross-sections at the central interface, (a3–d3) at the central interface after removal of the solidified Al drop.

with the increase of Si implantation dose. The ineffective elimination of oxide film (Al_2O_3) on the Cu-42.9Al drop surface brought about the no spreading or no wetting of Cu-42.9Al/(Si-)SiC systems. With the Al concentration increasing from 42.9 to 48.7, 70.4 and 100, the equilibrium contact angle was decreased from ~135° to ~50°, 40° and <7°, the early stabilization stage was shorted and till disappeared and the spreading of the rapid spreading stage was speed up gradually. In particular, the interfacial characteristic of Cu–Al/(Si-)SiC systems evolved from serious graphitization, non-reactive, low-reactive and high-reactive interfaces with the Al concentration increasing from 0 to 42.9, 48.7, 70.4 and 100. The Si ion implantation can strengthen the interfacial reactions of Cu/SiC system, and enhance the formation of Al_4C_3 layer at the triple line of Cu-(70.4, 100)Al/SiC systems, which can affect the wettability of the corresponding system.

Declaration of competing interest

The authors declare that they have no known competing financial interests or personal relationships that could have appeared to influence the work reported in this paper.

CRediT authorship contribution statement

Yalong Zhu: Formal analysis, Writing - original draft. **Mingfen Zhang:** Formal analysis, Validation. **Xiangzhao Zhang:** Resources, Writing - review & editing. **Zhikun Huang:** Formal analysis. **Guiwu Liu:** Resources, Writing - review & editing. **Guanjun Qiao:** Resources, Supervision.

Acknowledgements

This research work is supported by the National Key R&D Program of China (2017YFB0310400), National Natural Science Foundation of China (51572112), Key R&D Plan (BE2019094) of Jiangsu Province, Natural Science Foundation (BK20151340) of Jiangsu Province, 333 talents project (BRA2017387) of Jiangsu Province, Qing Lan Project [(2016)15] of Jiangsu Province and Six Talent Peaks Project (TD-XCL-004) of Jiangsu Province.

References

[1] Y.H. Huang, D.L. Jiang, X.F. Zhang, Z.K. Liao, Z.R. Huang, Enhancing toughness and strength of SiC ceramics with reduced graphene oxide by HP sintering, J. Eur. Ceram. Soc. 38 (13) (2018) 4329–4337, https://doi.org/10.1016/j.jeurceramsoc.2018.05.033.

[2] J.B. Casady, R.W. Johnson, Status of silicon carbide (SiC) as a wide-bandgap semiconductor for high-temperature applications: a review, Solid State Electron. 39 (10) (1996) 1409–1422, https://doi.org/10.1016/0038-1101(96)00045-7.

[3] T. Tsunoura, K. Yoshida, T. Yano, T. Aoki, T. Ogasawara, Oxidation mechanisms of SiC-fiber–reinforced Si eutectic alloy matrix composites at elevated temperatures, J. Am. Ceram. Soc. 102 (10) (2019) 6309–6321, https://doi.org/10.1111/jace.16487.

[4] G.W. Liu, F. Valenza, M.L. Muolo, A. Passerone, SiC/SiC and SiC/Kovar joining by Ni-Si and Mo interlayers, J. Mater. Sci. 45 (16) (2010) 4299–4307, https://doi.org/10.1007/s10853-010-4337-3.

[5] G.W. Liu, F. Valenza, M.L. Muolo, G.J. Qiao, A. Passerone, Wetting and interfacial behavior of Ni-Si alloy on different substrates, J. Mater. Sci. 44 (22) (2009) 5990–5997, https://doi.org/10.1007/s10853-009-3858-0.

[6] G.W. Liu, X.Z. Zhang, J. Yang, G.J. Qiao, Recent advances in joining of SiC-based materials (monolithic SiC and SiC_f/SiC composites): joining techniques, joint strength and interfacial behavior, J. Adv. Ceram. 8 (1) (2019) 19–38, https://doi.org/10.1007/s40145-018-0297-x.

[7] S.T. Zhao, X.Z. Zhang, G.W. Liu, F. Valenza, M.L. Muolo, G.J. Qiao, A. Passerone, Wetting and interfacial behavior of molten Cu on Co-Si(-Mo) coated SiC, Ceram. Int. 41 (10) (2015) 13493–13501, https://doi.org/10.1016/j.ceramint.2015.07.141.

[8] S. Gambaro, F. Valenza, G. Cacciamani, M.L. Muolo, A. Passerone, F. Toche, R. Chiriac, O. Dezellus, High-Temperature-Reactivity of Al-Ti alloys in contact with SiC, J. Alloys Compd. (2019), https://doi.org/10.1016/j.jallcom.2019.152715 in press.

[9] K. Zhang, Z.Q. Shi, H.Y. Xia, K. Wang, G.W. Liu, G.J. Qiao, J.F. Yang, Preparation and thermophysical properties of directional SiC/Cu–Si composite via spontaneous infiltration, Ceram. Int. 42 (1) (2016) 996–1001, https://doi.org/10.1016/j.ceramint.2015.08.173.

[10] X.S. Cong, P. Shen, Y. Wang, Q.C. Jiang, Wetting of polycrystalline SiC by

molten Al and Al-Si alloys, Appl. Surf. Sci. 317 (2014) 140–146, https://doi.org/10.1016/j.apsusc.2014.08.055.
[11] P. Shen, Y. Wang, L. Ren, S.X. Li, Y.H. Liu, Q.C. Jiang, Influence of SiC surface polarity on the wettability and reactivity in an Al/SiC system, Appl. Surf. Sci. 355 (2015) 930–938, https://doi.org/10.1016/j.apsusc.2015.07.164.
[12] Z.K. Huang, X.Z. Zhang, T.T. Wang, G.W. Liu, H.C. Shao, Y.G. Wan, G.J. Qiao, Effects of Pd ion implantation and Si addition on wettability of Al/SiC system, Surf. Coat. Technol. 335 (2018) 198–204, https://doi.org/10.1016/j.surfcoat.2017.12.027.
[13] C. Rado, B. Drevet, N. Eustathopoulos, The role of compound formation in reactive wetting: the Cu/SiC system, Acta Mater. 48 (18–19) (2000) 4483–4491, https://doi.org/10.1016/S1359-6454(00)00235-4.
[14] Q. An, X.S. Cong, P. Shen, Q.C. Jiang, Roles of alloying elements in wetting of SiC by Al, J. Alloys Compd. 784 (2019) 1212–1220, https://doi.org/10.1016/j.jallcom.2019.01.138.
[15] S.T. Zhao, F. Valenza, G.W. Liu, M.L. Muolo, G.J. Qiao, A. Passerone, Surface characterization of Mo-implanted 6H-SiC by high temperature non-reactive wetting tests with the Ni–56Si alloy, Ceram. Int. 40 (5) (2014) 7227–7234, https://doi.org/10.1016/j.ceramint.2013.12.062.
[16] J. Wong-Leung, M.K. Linnarsson, B.G. Svensson, D.J.H. Cockayne, Ion-implantation-induced extended defect formation in (0001) and (1120) 4H-SiC, Phys. Rev. B 71 (16) (2005) 165210, https://doi.org/10.1103/PhysRevB.71.165210, 1–13.
[17] T.T. Wang, G.W. Liu, Z.K. Huang, X.Z. Zhang, Z.W. Xu, G.J. Qiao, Wettability of Si and Al-12Si alloy on Pd-implanted 6H-SiC, Chin. Phys. B 27 (4) (2018) 352–356, https://doi.org/10.1088/1674-1056/27/4/046101.
[18] Z.K. Huang, W.L. Xu, G.W. Liu, T.T. Wang, X.Z. Zhang, G.J. Qiao, Wetting and interfacial behavior of molten Al–Si alloys on SiC monocrystal substrates: effects of Cu or Zn addition and Pd ion implantation, J. Mater. Sci. Mater. Electron. 29 (20) (2018) 17416–17424, https://doi.org/10.1007/s10854-018-9839-9.
[19] Z.K. Huang, H. Liu, G.W. Liu, T.T. Wang, X.Z. Zhang, J. Wu, Y.G. Wan, G.J. Qiao, Influences of surface polarity and Pd ion implantation on the wettability of Al-12Si(-2Mg)/SiC systems, Mater. Chem. Phys. 211 (2018) 329–334, https://doi.org/10.1016/j.matchemphys.2018.02.028.
[20] N. Eustathopoulos, N. Sobczak, A. Passerone, K. Nogi, Measurement of contact angle and work of adhesion at high temperature, J. Mater. Sci. 40 (9–10) (2005) 2271–2280, https://doi.org/10.1007/s10853-005-1945-4.
[21] T.T. Wang, Z.W. Xu, X.Z. Zhang, G.W. Liu, G.J. Qiao, Formation mechanism of multivacancies on H-passivated and Si-reconstructed surfaces of 6H-SiC (0001): a DFT calculation, Mater. Res. Express 5 (10) (2018) 1–8, https://doi.org/10.1088/2053-1591/aad955.
[22] X.B. Li, Z.Z. Chen, E.W. Shi, Effect of doping on the Raman scattering of 6H-SiC crystals, Phys. B 405 (10) (2010) 2423–2426, https://doi.org/10.1016/j.physb.2010.02.058.
[23] K.F. Domke, B. Pettinger, Tip-enhanced Raman spectroscopy of 6H-SiC with graphene adlayers: selective suppression of E1 modes, J. Raman Spectrosc. 40 (10) (2010) 1427–1433, https://doi.org/10.1002/jrs.2434.
[24] S.H. Lin, Z.M. Chen, L.B. Li, C. Yang, Effect of impurities on the Raman scattering of 6H-SiC Crystals, Mater. Res. 15 (6) (2012) 833–836, https://doi.org/10.1590/S1516-14392012005000108.
[25] X.F. Chen, W. Zhou b, Q.J. Feng, J. Zheng, X.K. Liu, B. Tang, J.B. Li, J.M. Xue, S.M. Peng, Irradiation effects in 6H-SiC induced by neutron and heavy ions: Raman spectroscopy and high-resolution XRD analysis, J. Nucl. Mater. 478 (2016) 215–221, https://doi.org/10.1016/j.jnucmat.2016.06.020.
[26] P. Morgen, U. Hofer, W. Wurth, E. Umbach, Initial stages of oxygen adsorption on Si (111): the stable state, Phys. Rev. B 39 (6) (1989) 3720–3734, https://doi.org/10.1103/PhysRevB.39.3720.
[27] Y. Igari Kusunoki, XPS study of a SiC film produced on Si (100) by reaction with a C_2H_2 beam, Appl. Surf. Sci. 59 (2) (1992) 95–104, https://doi.org/10.1016/0169-4332(92)90293-7.
[28] D.F. Mitchell, K.B. Clark, J.A. Bardwell, W.N. Lennard, G.R. Massoumi, I.V. Mitchell, Film thickness measurements of SO_2 by XPS, Surf. Interface Anal. 21 (1994) 44–50, https://doi.org/10.1002/sia.740210107.
[29] P. Shen, H. Fujii, K. Nogi, Wetting, adhesion and diffusion in Cu–Al/SiO_2 system at 1473 K, Scripta Mater. 52 (12) (2005) 1259–1263, https://doi.org/10.1016/j.scriptamat.2005.02.019.
[30] G.W. Liu, M.L. Muolo, F. Valenza, A. Passerone, Survey on wetting of SiC by molten metals, Ceram. Int. 36 (4) (2010) 1177–1188, https://doi.org/10.1016/j.ceramint.2010.01.001.
[31] Contreras, Wetting of TiC by Al–Cu alloys and interfacial characterization, J. Colloid Interface Sci. 311 (1) (2007) 159–170, https://doi.org/10.1016/j.jcis.2007.02.041.
[32] G.R. Prin, T. Baffie, M. Jeymond, N. Eustathopoulos, Contact angles and spreading kinetics of Al and Al–Cu alloys on sintered AlN, Mater. Sci. Eng., A 298 (1–2) (2001) 34–43, https://doi.org/10.1016/S0921-5093(00)01317-4.
[33] A.T. Dinsdale, P.N. Quested, The viscosity of aluminium and its alloys-A review of data and models, J. Mater. Sci. 39 (24) (2004) 7221–7228, https://doi.org/10.1023/b:jmsc.0000048735.50256.96.
[34] N.Yu Konstantinova, P.S. Popel, D.A. Yagodin, The kinematic viscosity of liquid copper-aluminum alloys, High Temp. 47 (3) (2009) 336–341, https://doi.org/10.1134/s0018151x09030067.
[35] R.I.L. Guthrie, T. Iida, Thermodynamic properties of liquid metals, Mater. Sci. Eng., A 178 (1–2) (1994) 35–41, https://doi.org/10.1016/0921-5093(94)90515-0.